COMMUNICATION

Well-Defined Multibranched Gold with Surface Plasmon Resonance in Near-Infrared Region from Seeding Growth Approach Using Gyroid Block Copolymer Template

*Han-Yu Hsueh, Hung-Ying Chen, Yu-Chueh Hung, Yi-Chun Ling, Shangjr Gwo, and Rong-Ming Ho**

Nanostructural and morphological designs of metals have attracted intensive attention because of their effectiveness in tuning electronic, optical, magnetic, and catalytic properties.[1] In particular, synthesis of nanostructured gold (Au) with controllable size and shape has become the critical aim of extensive research over the last few years due to the unique properties of the nanostructured Au, such as chemical stability, high conductivity, catalytic activity,[2,3] and surface plasmon resonance (SPR).[4,5] Nanostructured Au with highly branched morphology that absorbs and scatters in the near-infrared region (NIR, 760–1400 nm) can exhibit strong enhancement of an electromagnetic field leading to surface enhanced Raman scattering (SERS) for biomedical applications.[6,7] Most of the work focus on the synthesis of Au nanoobjects such as sphere, cube, plate, rod and branched texture in aqueous solution.[1,5–16] Xia and coworkers demonstrated the control of the shape of metallic nanoparticles by chemical synthesis from aqueous solution for exploiting their properties and corresponding applications.[1] For the applications of SPR materials, it is often to require the materials possessing mechanically robust and chemically stable properties. As a result, how to assemble those SPR materials giving self-supporting materials as large-size bulks and large-area continuous films remains challenge.

Prof. R.-M. Ho
Department of Chemical Engineering
National Tsing Hua University
Hsinchu 30013, Taiwan
Frontier Research Center on Fundamental and Applied Sciences of Matters;
Department of Chemical Engineering
National Tsing Hua University
Hsinchu 30013, Taiwan
E-mail: rmho@mx.nthu.edu.tw
Dr. H.-Y. Hsueh
Department of Chemical Engineering
National Tsing Hua University
Hsinchu 30013, Taiwan
Dr. H.-Y. Chen, Prof. Dr. S. Gwo
Department of Physics
National Tsing Hua University
Hsinchu 30013, Taiwan
Prof. Dr. Y.-C. Hung, Y.-C. Ling
Institute of Photonics Technologies
National Tsing Hua University, Hsinchu 30013, Taiwan

DOI: 10.1002/adma.201204631

One easy way to fulfill the requirements is to acquire it through templated synthesis. A straightforward route to fabricate nanostructures with predefined size and shape has been developed by deposition of metals into templates with desired channels, such as anodized aluminum oxide films (AAO),[17] arrays of colloidal crystals,[18] and mesoporous silica (MCM materials).[19] In recent decades, block copolymers (BCPs) have been extensively investigated because of their ability to self-assemble into one-, two-, and three-dimensional (3D) periodic nanostructures with readily adjustable size, depending on their constituted compositions and molecular weights.[20] By taking advantage of the degradable character of BCPs, nanoporous polymer materials with well-ordered textures can be prepared by preferential removal of constituted components in BCPs through ozonolysis,[21] UV degradation,[22] and reactive ion etching.[23] As a result, chemically degradable BCPs have drawn intensive attention for the preparation of nanoporous polymers. Also, polylactide-containing BCPs (such as polystyrene-*b*-poly(D,L-lactide) (PS-PLA)[24] and polystyrene-*b*-poly(L-lactide) (PS-PLLA)[25,26]) are highly suitable for the fabrication of nanoporous polymers because of the unstable character of ester group in polylactides, which can be hydrolytically degenerated. Most interestingly, the nanoporous polymers with well-defined nanochannels can be used as templates for templated synthesis. By exploiting the templating process, reactions, such as electrochemical deposition,[27–29] electroless plating,[30,31] and sol-gel reaction,[32,33] can be carried out within the BCP templates for the manufacture of nanostructured inorganic materials with precisely-controlled textures after removal of the polymer template. For the fabrication of 3D and complex Au nanostructures with high branches, the double gyroid (DG), which is a unique geometry, is an appealing morphology to serve the purposes. The DG morphology is composed of a matrix and two continuous, interpenetrating but independent networks in 3D space.[34–36] The basic shape of the gyroid is a three-fold junction of three arms, in which each arm connects to another set of three arms that are each themselves rotated to form a 3D network. Therefore, after the selective degradation of the minor phase, the DG nanostructure can be exploited to create fully interconnected nanochannels leading to great potential for fabrication of branched nanostructures as the nanochannels are occupied by specific materials.

Here, we develop a new approach to fabricate multibranched Au with well-defined textures as bulks or continuous thin films by using gyroid-forming nanoporous polymer as a template for templated seeding growth approach, followed by removal

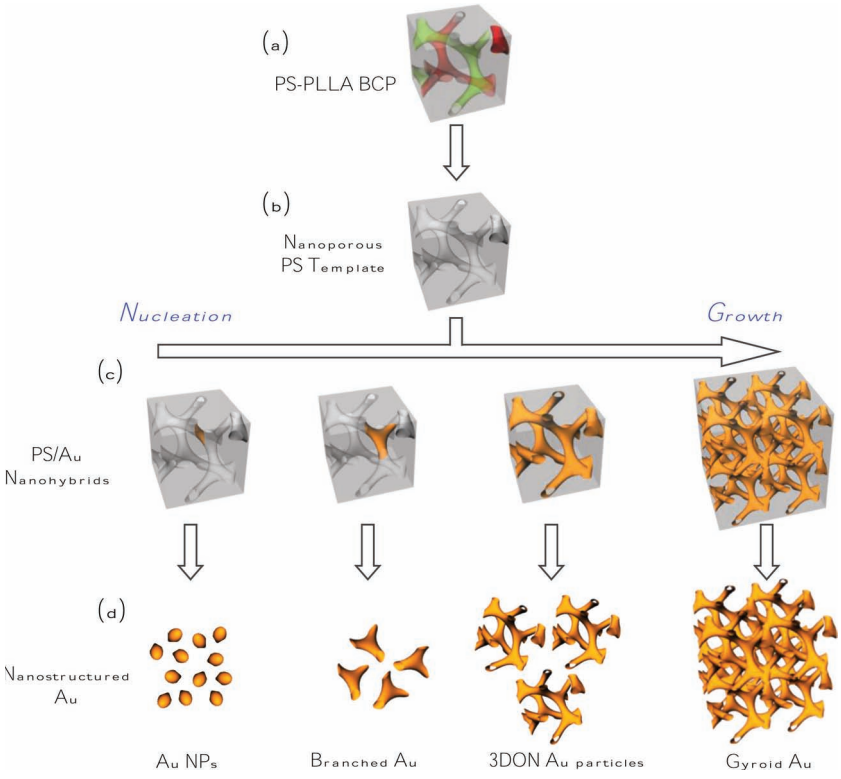

Figure 1. Schematic illustration for fabrication of well-defined nanostructured Au from BCP template: a) PS-PLLA DG phase (skeleton of DG structure with two identical networks (green and red)); b) Gyroid-forming nanoporous PS template after removal of PLLA network; c) PS/Au nanohybrids from controlled nucleation and growth of Au within the BCP template *via* seeding growth approach; d) Nanostructured Au after removal of PS template.

of the template. **Figure 1** shows the schematic illustration of the templated seeding growth approach for fabricating nanostructured gold using BCP as a template. A PS-PLLA BCP with a PLLA volume fraction of 39% was synthesized (see Supporting Information for details).[33] A DG phase consisting of co-continuous PLLA networks in a PS matrix can be formed after solution casting of the synthesized PS-PLLA followed by quenching from the microphase-separated melt. One-dimensional small-angle X-ray scattering (1D SAXS) profile confirms the DG phase. After hydrolytic treatment, the PLLA networks can be selectively removed to give a PS matrix possessing interconnected air networks as a template for the nucleation and growth of Au through seeding growth approach (see Figure S1 for details). The corresponding TEM images of the microsection of the PS-PLLA BCP and the nanoporous PS template with gyroid-forming nanochannels can be observed as shown in Figure S2.

The size and periods of the microphase-separated nanostructures from the self-assembly of BCPs are adjustable by tuning the molecular weight and composition of the PS-PLLA used. As a result, it is possible to create nanoporous gyroid materials with different pore sizes ranging from ten to fifty nanometers and various periods by using various gyroid-forming PS-PLLA.[26] Subsequently, various nanostructured Au within the nanochannels of PS template can be synthesized by controlling the growth time of forming Au, leading to the formation of organic/inorganic (i.e., PS/Au) nanohybrids. As a result, versatile nanostructured Au, such as Au nanoparticle (NP), branched Au, three-dimensionally ordered nanoporous Au (3DON Au) particle and nanoporous gyroid Au can be successfully fabricated after removal of the PS matrix by UV-ozonolysis or dissolution using tetrahydrofuran (THF).

Seeding growth approach is a chemical deposition process, which depends upon the self-catalytic reduction of metal ions in an aqueous solution containing a chemical reducing agent. Seeding growth usually experiences two steps: synthesis of seeds (nuclei) and growth of seeds. Cetyltrimethylammonium bromide is used as a protector, which allows the anisotropic growth of nanostructured Au. Also, a low concentration of Ag ions (Ag^+) must be present to fabricate nanostructured Au with high aspect ratios.[12] In contrast to the classical seeding growth process, the templated seeding growth for synthesis of nanostructured Au provides the advantage of simple operation and the ease of controlling the size and shape of Au without any surfactants and additional ions. Moreover, unlike electrochemical deposition, the process of nucleation and growth for metal deposition in this study is not necessary to pass any electric current through the solution to form a deposit; namely, there is no need to use conductive substrates to fabricate nanostructured metals. This templated seeding growth approach can be conducted under ambient conditions to create well-defined multibranched Au with nanoscaled size, specific shape, and uniform distribution in a PS matrix with remarkable SPR property in NIR region, which can have significant applications for biological research.

For the nucleation process of Au seeds, the nanoporous PS template is soaked in an aqueous Au ion (Au^{+3}) solution mixed with methanol. Methanol is used to enhance the wetting tendency of the precursor solution into the PS templates through capillary force. The porous template with the nanopores filled with Au ion solution is then immersed into a mixed aqueous solution of methanol and hydrazinium hydroxide (N_2H_5OH) (a strong reducing agent for the Au ions) at room temperature. Immediately, the nucleation of Au seeds can be initialized at which Au ions can be reduced to Au nuclei by N_2H_5OH. **Figure 2**a shows the TEM micrograph of the Au NPs (Au nuclei) from nucleation of Au (500 ppm $HAuCl_4$ in methanol). The nucleation density can be calculated from the results of TEM cross section, and the nucleation density is estimated as 7.0×10^6 nuclei per cubic centimeter (cm^3). The diameter of Au nuclei is approximately 28 nm as determined from the TEM results, indicating the well preservation of the size of template. After removal of PS template, Au NPs can be well dispersed on the silicon wafer as shown in **Figure 3**a. To achieve the successful templating, it is necessary to introduce the metal ions in advance to the occurrence of metal deposition

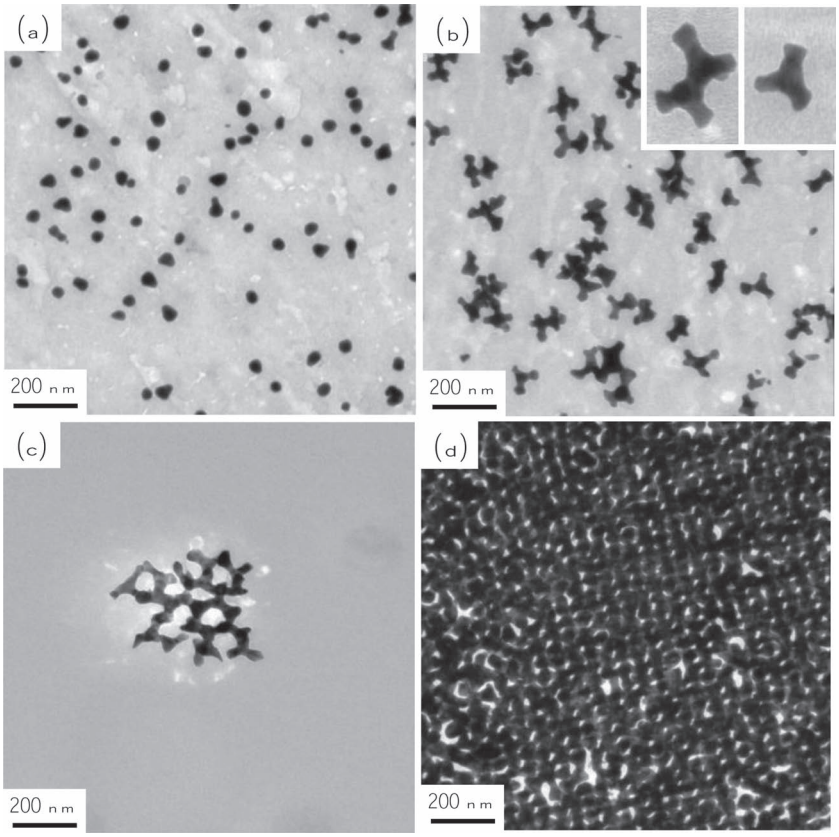

Figure 2. TEM images of nanostructured Au from controlled nucleation and growth of Au within the BCP template *via* templated seeding growth approach at different stages: a) Au NPs (Au nuclei) from nucleation of Au with higher Au ion concentrations (500 ppm $HAuCl_4$ in methanol); b) Branched Au from the growth process of Au nuclei for 6 hours. The inset shows the enlarged area; c) 3DON Au particles from the growth of Au nuclei with low seeding density from nucleation of Au with lower Au ion concentrations (50 ppm $HAuCl_4$ in methanol) after 24 hour growth; d) Gyroid Au from the growth of 3DON Au particles after 3 day growth.

so as to carry out templated seeding growth approach for the formation of nanostructured metals. Therefore, weak reducing agents (i.e., diethanolamine (DEA)) are used (see Figure S3 for details) for growth process. Figure 2b shows the branched Au from the templated growth process for 6 hours using the same seeding density with the one in Figure 2a. In contrast to Figure 2a, the growth of Au gives the formation of multipod texture with three-fold symmetry as expected by using the gyroid-forming nanochannels as a template. However, dual populations of nanostructured Au, including Au spheres and branched Au, were obtained (Figure S4a). To acquire branched Au only, the nucleation behavior of Au was adjusted by using low concentration of added chloride ion (Cl^-) so that the nucleation density of Au can be well controlled to give heterogeneous nucleation (i.e., constant nucleation density) for the following growth. By taking into account that $HAuCl_4$ is used as a precursor of Au reduction, chloride ions are present in the reaction mixture and could inhibit the nucleation and growth of Au, leading to the growth of narrow size distribution of branched Au at suitable concentration of chloride ions.[37,38] As a result, single population of branched Au nanostructures with well-defined texture can be obtained (Figure S4b).

Following the growth of Au nanostructures, continuous reduction of Au ions can be homogeneously conducted with the reduction time. Consequently, 3DON Au particles in a polymer matrix can be formed. Although the templated synthesis of nanostructured Au can be well conducted to give the controlled size and shape of the nanostructured Au, the clusters of Au nanostructures (i.e., 3DON Au particles) appear different size as shown in Figure S5. The formation of irregular textures of the 3DON Au particles is attributed to the high initial nucleation density for the growth of the Au ions at which the growth of the Au nanostructures might be blocked by the neighboring clusters, resulting in the area with remaining nanochannels (indicated by an arrow in Figure S5) caused by the limited diffusion due to the blocking described above. As a result, the nanostructured Au with low density of Au nuclei should be used as seeds for the following growth of Au. The seeding density of Au can be easily adjusted by controlling the concentration of Au ions as shown in Figure S6 at which the seeding density of Au indeed increases with the initial concentration of Au ions. Figure 2c shows the TEM micrograph of 3DON Au particles from the growth of Au nuclei with low seeding density from nucleation of Au with lower Au ion concentrations (50 ppm $HAuCl_4$ in methanol) after 24 hours. The nucleation density is estimated as 2.5×10^4 nuclei per cubic centimeter. Because of sufficient diffusion for material exchange and the continuous growth of Au, 3DON Au particles, and the embryonic form of gyroid nanostructure with three-fold symmetry, can be clearly recognized. After removal of PS template, branched Au and 3DON Au particles with well-defined textures can be manufactured as shown in Figures 3b and 3c, respectively. Obviously, the advantage of the templated seeding growth approach is for the fabrication of well-ordered branched Au and 3DON Au particles, which can be hardly synthesized by other approaches.

As the growth time of 3DON Au particles is further increased, the gyroid Au nanostructure can be successfully formed in the PS matrix as shown in Figure 2d. Figure 3d displays the field emission SEM (FESEM) microscopy image of the gyroid Au in the PS/Au gyroid nanohybrids after removal of the PS template. The texture of nanoporous gyroid Au with three-fold symmetry can be clearly recognized, indicating that the bicontinuous materials with precisely controlled pore geometries can be well fabricated. The XRD results of the nanoporous gyroid Au are shown in Figure 3e. All the diffractions can be indexed as fcc Au with the lattice constant a = 4.080 Å, JCPDS card no. 04-0784, corresponding to the reflections from (111), (200), (220), (311) and (222) planes. The intrinsic density of pure Au without pores *via* the seeding growth approach is approximately 18.0 g cm^{-3} from our measurement. The porosity of the gyroid Au is around 61%

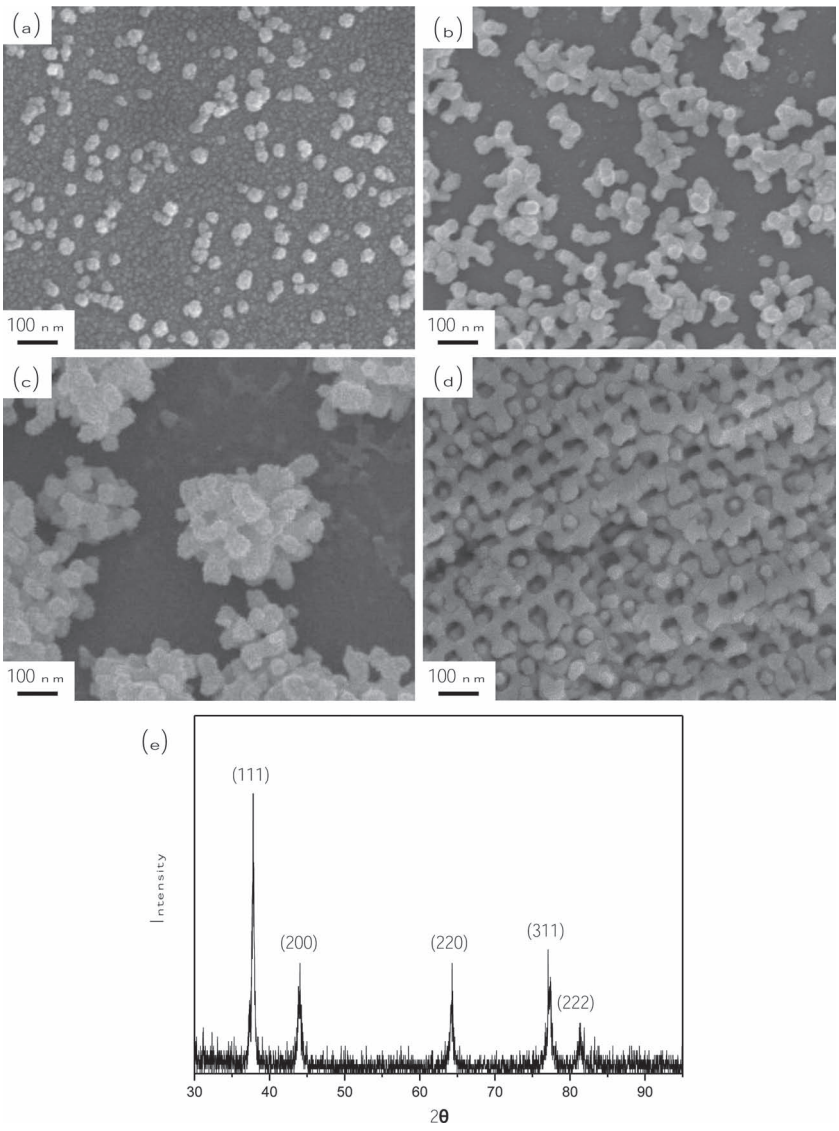

Figure 3. FESEM microscopy images of nanostructured Au from PS/Au nanohybrids after removal of PS template: a) Au NPs (Au nuclei) from nucleation of Au (III) ions with higher Au ion concentrations (500 ppm $HAuCl_4$ in methanol); b) Branched Au from the growth process of Au nuclei with high seeding density for 6 hours; c) 3DON Au particles from the growth of Au nuclei with low seeding density after 24 hour growth; d) Nanoporous gyroid Au from the growth of 3DON Au particles after 3 day growth. All of the nanostructured Au were obtained after removal of the PS matrix by exposure to UV-O_3. (e) One-dimensional XRD profiles of the nanoporous gyroid Au.

calculated on the basis of the composition of the PS-PLLA used. As a result, the density of gyroid Au is approximately 7.02 g cm^{-3} (39% relative density). On the basis of the constituted volume fraction of the PS block (61%), it is expected to have the nanoporous gyroid Au possess high specific surface area and high porosity after removal of the PS template. By assuming that the surface area of the inner wall of nanoporous PS template is theoretically the same with the outer wall of nanoporous gyroid Au, the specific surface area of nanoporous gyroid Au can be approximately estimated on the BET results of nanoporous PS template (97 m^2 g^{-1}). The density of nanoporous PS template is approximately 0.62 g cm^{-3} (61% relative density), and that of nanoporous gyroid Au is approximately 7.02 g cm^{-3} (39% relative density). Therefore, the specific surface area of nanoporous gyroid Au can be calculated as around 1693.91 m^2 mol^{-1} (8.6 m^2 g^{-1}). Note that the gyroid Au synthesized by templated seeding growth approach remains defects because it is difficult to completely fill the pores due to diffusion limitation. For 3D architecture with gyroid nanostructure, electrochemical deposition is a feasible method to fulfill the requirements to obtain well-ordered Au with long-range order by deposition of Au in gyroid-forming polymer template.[28] In addition, nanoporous Au fabricated *via* selective removal of Ag from Au-Ag alloy has been well developed.[39–43] The feature size in nanoporous Au can be controlled over a wide range from 10 nm to the micrometer length scale through an annealing procedure. Nevertheless, the structure of the nanoporous Au materials from dealloying is lack of order although they do exhibit well-distributed pore size.

The localized surface plasmon resonances (LSPR) are sensitively dependent upon the composition, size, shape, and environmental dielectric media of metallic materials. To obtain the plasmonic properties of various nanostructured Au prepared *via* the templated seeding growth approach, the plasmon resonances were characterized by optical absorption measurement. To precisely control the sample thickness (i.e., 200 nm as measured by alpha-step profilometer), testing samples for the following experiments were obtained by ultramicrotomy from the bulk samples and then transferred onto quartz substrates. **Figure 4** shows the experimental and simulated results for the four types of nanostructured Au. The UV-Vis absorption spectra were obtained using a homemade optical microscope with a 100× objective lens (Olympus, MPlan, N.A. = 0.9). For the simulation, finite-difference time-domain (FDTD) method was used to calculate the absorption spectra of versatile nanostructured Au under the excitation of non-polarized light. Lorentz-Drude model was used to model the dispersion and loss properties of Au.[44] The dimension of a unit cell of DG network was determined as 100 nm × 100 nm × 100 nm, as estimated from the SAXS results (Figure S1), and the volume fraction was 39% according to the fabrication parameter. The Au seeds (Au NPs) with a diameter of 28 nm show a single LSPR peak at a wavelength of 538 nm, similar to the simulation result as shown in Figure 4a. The simulation result from Mie theory is also well consistent with the experimental and simulated results as shown in Figure S7, indicating the optical measurement and analysis of nanostructured Au are reliable. As the Au NPs grow to form branched

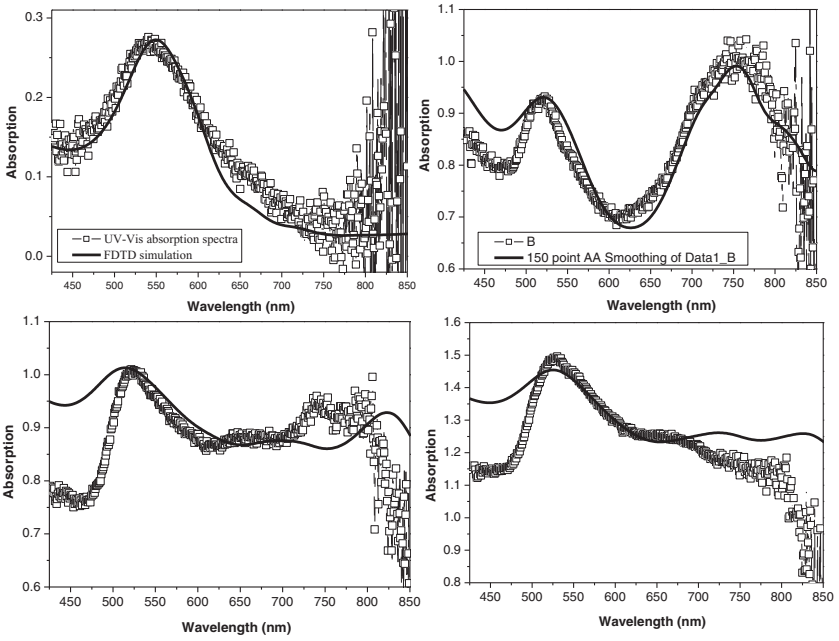

Figure 4. UV-Vis absorption spectra (blank squares) and FDTD simulation (solid lines) of nanostructured Au materials within the PS template with thickness of 200 nm *via* templated seeding growth approach at different stages: a) Au NPs; b) Branched Au; c) 3DON Au particles; d) Gyroid Au.

Au, the plasmon absorption will be split into two peaks at 518 and 756 nm (Figure 4b). Note that dipole plasmon resonance of anisotropic nanostructures such as nanorod is typically split into transverse and longitudinal dipole resonances because of the different dimensions along the width and length of the nanostructures.[45] Therefore, the peak centered at 756 nm in Figure 4b is likely a similar longitudinal plasmon resonance due to the elongated tips of the branched Au. By contrast, the 518 nm peak should represent the transverse plasmon resonance of the tips, which is also seen for Au nanostars in the solution.[46] Meanwhile, the branched Au shows a broadened absorption spectrum extending from the visible to NIR. Figure 4c presents the absorption spectrum of the 3DON Au particles. The structure of the 3DON Au particles can be seen as the combined products composed of a variety of branched Au with various angles so that the ensemble absorption of 3DON Au particles appears as a shoulder peak ranging from 600 to 800 nm because of the overlapping spectra from a variety of branched Au. Therefore, simulation for 3DON Au particles become much more difficult to be fitted with the experimental result due to the distribution of nanostructured Au fabricated. As shown in Figure 4c, the profile of simulation is similar to the experimental result but presents slight red shift, resulting from the mismatch of the structure and polarization direction between experiments and simulation. Furthermore, the 3DON Au particles give a strong absorption at 525 nm as compared to the branched Au. We speculate that the enhancement of the 525 nm absorption is attributed to the formation of the gyroid Au (see below for details).

Note that NIR is so-called "optical window" in biological tissue so that the well-defined multibranched Au (i.e., branched Au and 3DON Au particles) can be further used in biomedical applications. Also, the PS/Au nanohybrids (i.e., well-defined multibranched Au in a PS matrix) can be easily fabricated for device design because of easy processing for polymeric materials. For instance, different coating processes, such as slot and gravure coatings, can be applied to give cost-effective approaches for forming large-area thin films, and then used as templates for following seeding growth of Au to form thin-film SPR materials (**Figure 5**a). Branched Au and 3DON Au particles with uniform distribution in a large area on the substrate can be shown in Figures 5b and 5c, respectively. By taking advantage of the uniform distribution of the branched Au and 3DON Au particles in the PS matrix, a well-defined surface with strong SPR in the NIR region can be fabricated for bio-applications, and the applied work is in progress. Moreover, after removal of the PS matrix, 3DON Au particles are of particular interest for catalysis and

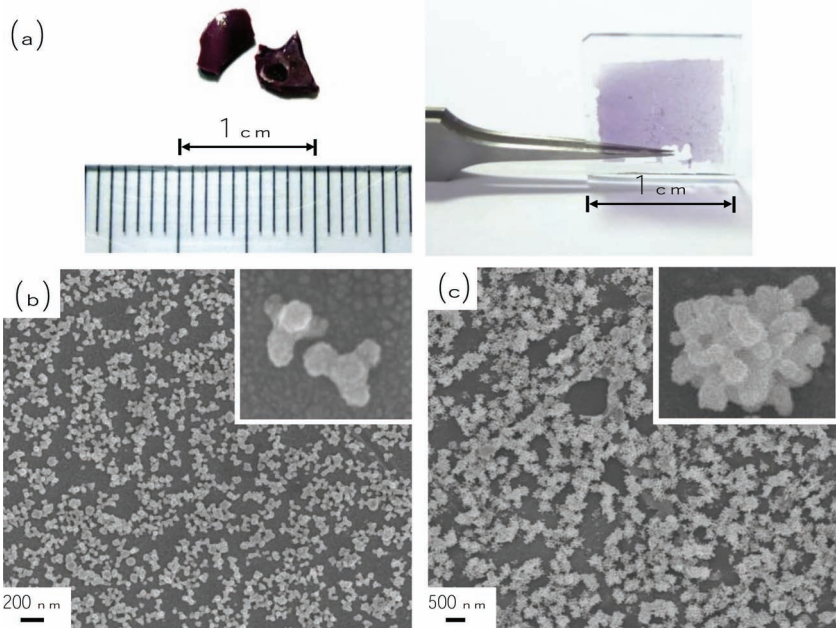

Figure 5. a) The photograph of well-defined multibranched Au in centimeter-sized PS bulk and thin film matrix with purple color. FESEM micrographs of b) branched Au and c) 3DON Au particles with uniform distribution in a large area on the substrate from PS/Au nanohybrids after removal of the PS template. Insets show the enlarged area.

drug deliver due to their large specific surface area and high specific activity for stepped atoms present on their branches. By combining the NIR plasmonic and biocompatible properties, the 3DON Au particles are potentially photothermal therapy agents for cancer target therapy. Also, as mentioned above, we speculate that the enhancement of the 525 nm absorption is attributed to the formation of the gyroid Au. The gyroid Au has an extremely strong absorption at 525 nm compared with other types of nanostructured Au (Figure 4d). Most interestingly, the NIR plasmon from 650 nm to 800 nm diminishes resulting from the reduction in the density of nanostructured edges (Figure S8). The discrepancy between the simulation and experimental results at higher wavelength (higher than 650 nm) might be attributed to the defects of grain boundaries from BCP self-assembly and voids from the incomplete Au growth in the nanochannels during the manufacturing process.

In conclusion, nanoporous polymers with gyroid nanochannels can be fabricated from the self-assembly of degradable BCPs, PS-PLLA, followed by the hydrolysis of PLLA blocks. A variety of well-defined Au nanostructures, such as Au NPs, branched Au, 3DON Au particles, and gyroid Au can be synthesized by using the nanoporous PS as a template for seeding growth approach. This templated seeding growth approach can be conducted under ambient conditions to create various nanostructured Au with remarkable SPR property. Particularly, the optical properties for branched Au and 3DON Au particles provide strong and stable NIR resonances that are appealing in biological applications. Note that metallic materials such as silver have superior SPR but is predisposed to oxidation resulting in problems with long-term storage. These polymer/metal nanohybrids allow the fabrication of optical-plasmonic devices with mechanical robustness and chemical stability so as to provide protection from the surrounding environments. Also, after removal of the PS matrix, versatile nanostructured Au with the nature of nanosized metals and the unique material characteristics of well-defined texture can be successfully fabricated for many applications, such as photonic crystals, metamaterials, SERS, catalysts and sensors. This new approach for BCP templating provides a precisely controlled method to fabricate nanohybrids and nanostructured metals for applications.

Experimental Section

The PS-PLLA BCP was prepared by a double-headed polymerization sequence. The PS-PLLA ($M_{n,PS}$ = 34000 g mol^{-1}, $M_{n,PLLA}$ = 27000 g mol^{-1}, polydispersity index (PDI) = 1.21, $f_{PLLA}{}^{v}$ = 0.39) was prepared by solution casting from dichloromethane (CH_2Cl_2) solution (10 wt% of PS-PLLA) at room temperature. After quenching from microphase-separated ordered melt, the PLLA blocks of the PS-PLLA bulk samples were removed by hydrolysis. The nanoporous PS template was soaked in an seeding aqueous solution mixed with methanol (20 mL) and $HAuCl_4{\cdot}3H_2O$ (0.01–0.1 g) with stirring at room temperature for several hours (3–4 h). The pore-filled samples were immersed into a hydrazinium hydroxide (100%, hydrazine 85%)/methanol solution for the nucleation of Au. Subsequently, a fresh growth solution consisting of $HAuCl_4{\cdot}3H_2O$ (0.05 g), diethanolamine (DEA, 0.1 g), HCl (1N, 0.1 mL), and methanol (20 mL) was prepared and then the pre-treated template with low content of Au nuclei was immersed into the prepared solution. Accordingly, Au ions were reduced to Au clusters arising from pre-formed Au nuclei so as to gradually develop within the nanochannels through the growth process and eventually form the PS/Au nanohybrids with preserved gyroid texture.

Supporting Information

Supporting Information is available from the Wiley Online Library or from the author.

Acknowledgements

The authors would like to thank the National Science Council of the Republic of China, Taiwan, for financially supporting this research under Contract No. Grant NSC 101-2120-M-007-007-. The National Synchrotron Radiation Research Center (NSRRC) for its assistance in the Synchrotron SAXS experiments.

Received: November 8, 2012
Published online: January 29, 2013

[1] Y. N. Xia, Y. J. Xiong, B. Lim, S. E. Skrabalak, *Angew. Chem. Int. Ed.* **2009**, *48*, 60–103.
[2] M. Haruta, *Gold Bull.* **2004**, *37*, 27–36.
[3] A. Wittstock, V. Zielasek, J. Biener, C. M. Friend, M. Baumer, *Science* **2010**, *327*, 319–322.
[4] S. Link, M. A. El-Sayed, *J. Phys. Chem. B* **1999**, *103*, 8410–8426.
[5] Y. N. Xia, N. J. Halas, *MRS Bulletin* **2005**, *30*, 338–344.
[6] E. Hao, R. C. Bailey, G. C. Schatz, J. T. Hupp, S. Y. Li, *Nano Lett.* **2004**, *4*, 327–330.
[7] O. M. Bakr, B. H. Wunsch, F. Stellacci, *Chem. Mater.* **2006**, *18*, 3297–3301.
[8] C. C. Li, K. L. Shuford, Q. H. Park, W. P. Cai, Y. Li, E. J. Lee, S. O. Cho, *Angew. Chem. Int. Ed.* **2007**, *46*, 3264–3268.
[9] D. Seo, J. C. Park, H. Song, *J. Am. Chem. Soc.* **2006**, *128*, 14863–14870.
[10] X. P. Sun, S. J. Dong, E. Wang, *Angew. Chem. Int. Ed.* **2004**, *43*, 6360–6363.
[11] N. R. Jana, L. Gearheart, C. J. Murphy, *J. Phys. Chem. B* **2001**, *105*, 4065–4067.
[12] S. H. Chen, Z. L. Wang, J. Ballato, S. H. Foulger, D. L. Carroll, *J. Am. Chem. Soc.* **2003**, *125*, 16186–16187.
[13] Z. Q. Li, W. Y. Li, P. H. C. Camargo, Y. N. Xia, *Angew. Chem. Int. Ed.* **2008**, *47*, 9653–9656.
[14] H. G. Liao, Y. X. Jiang, Z. Y. Zhou, S. P. Chen, S. G. Sun, *Angew. Chem. Int. Ed.* **2008**, *47*, 9100–9103.
[15] C. H. Kuo, M. H. Huang, *Langmuir* **2005**, *21*, 2012–2016.
[16] F. Hao, C. L. Nehl, J. H. Hafner, *Nano Lett.* **2007**, *7*, 729–732.
[17] R. C. Furneaux, W. R. Rigby, A. P. Davidson, *Nature* **1989**, *337*, 147–149.
[18] A. A. Zakhidov, R. H. Baughman, Z. Iqbal, C. X. Cui, I. Khayrullin, S. O. Dantas, I. Marti, V. G. Ralchenko, *Science* **1998**, *282*, 897–901.
[19] A. Monnier, F. Schuth, Q. Huo, D. Kumar, D. Margolese, R. S. Maxwell, G. D. Stucky, M. Krishnamurty, P. Petroff, A. Firouzi, M. Janicke, B. F. Chmelka, *Science* **1993**, *261*, 1299–1303.
[20] F. S. Bates, G. H. Fredrickson, *Annu. Rev. Phys. Chem.* **1990**, *41*, 525–557.
[21] M. Park, C. Harrison, P. M. Chaikin, R. A. Register, D. H. Adamson, *Science* **1997**, *276*, 1401–1404.
[22] T. Thurn-Albrecht, R. Steiner, J. DeRouchey, C. M. Stafford, E. Huang, M. Bal, M. Tuominen, C. J. Hawker, T. P. Russell, *Adv. Mater.* **2000**, *12*, 787–791.
[23] J. Y. Cheng, C. A. Ross, V. Z. H. Chan, E. L. Thomas, R. G. H. Lammertink, G. J. Vancso, *Adv. Mater.* **2001**, *13*, 1174–1178.

[24] A. S. Zalusky, R. Olayo-Valles, C. J. Taylor, M. A. Hillmyer, *J. Am. Chem. Soc.* **2001**, *123*, 1519–1520.
[25] R. M. Ho, W. H. Tseng, H. W. Fan, Y.-W. Chiang, C. C. Lin, B. T. Ko, B. H. Huang, *Polymer* **2005**, *46*, 9362–9377.
[26] R.-M. Ho, Y.-W. Chiang, C.-K. Chen, H.-W. Wang, H. Hasegawa, S. Akasaka, E. L. Thomas, C. Burger, B. S. Hsiao, *J. Am. Chem. Soc.* **2009**, *131*, 18533–18542.
[27] E. J. W. Crossland, M. Kamperman, M. Nedelcu, C. Ducati, U. Wiesner, D. M. Smilgies, G. E. S. Toombes, M. A. Hillmyer, S. Ludwigs, U. Steiner, H. J. Snaith, *Nano Lett.* **2009**, *9*, 2807–2812.
[28] S. Vignolini, N. A. Yufa, P. S. Cunha, S. Guldin, I. Rushkin, M. Stefik, K. Hur, U. Wiesner, J. J. Baumberg, U. Steiner, *Adv. Mater.* **2011**, *24*, OP23–OP27.
[29] M. R. J. Scherer, L. Li, P. M. S. Cunha, O. A. Scherman, U. Steiner, *Adv. Mater.* **2012**, *24*, 1217–1221.
[30] T. Hashimoto, K. Tsutsumi, Y. Funaki, *Langmuir* **1997**, *13*, 6869–6872.
[31] H. Y. Hsueh, Y. C. Huang, R. M. Ho, C. H. Lai, T. Makida, H. Hasegawa, *Adv. Mater.* **2011**, *23*, 3041–3046.
[32] W. H. Tseng, C. K. Chen, Y. W. Chiang, R. M. Ho, S. Akasaka, H. Hasegawa, *J. Am. Chem. Soc.* **2009**, *131*, 1356.
[33] a) H. Y. Hsueh, H. Y. Chen, M. S. She, C. K. Chen, R. M. Ho, S. Gwo, H. Hasegawa, E. L. Thomas, *Nano. Lett.* **2010**, *10*, 4994–5000; b) H. Y. Hsueh, R. M. Ho, *Langmuir* **2012**, *28*, 8518–8529.
[34] D. A. Hajduk, P. E. Harper, S. M. Gruner, C. C. Honeker, G. Kim, E. L. Thomas, L. J. Fetters, *Macromolecules* **1994**, *27*, 4063–4075.
[35] M. F. Schulz, F. S. Bates, K. Almdal, K. Mortensen, *Phys. Rev. Lett.* **1994**, *73*, 86–89.
[36] M. W. Matsen, M. Schick, *Phys. Rev. Lett.* **1994**, *72*, 2660–2663.
[37] T. H. Ha, H. J. Koo, B. H. Chung, *J. Phys. Chem. C* **2007**, *111*, 1123–1130.
[38] T. K. Sau, A. L. Rogach, *Adv. Mater.* **2010**, *22*, 1781–1804.
[39] J. Erlebacher, M. J. Aziz, A. Karma, N. Dimitrov, K. Sleradzki, *Nature* **2001**, *410*, 450–453.
[40] T. Fujita, L. H. Qian, K. Inoke, J. Erlebacher, M. W. Chen, *Appl. Phys. Lett.* **2008**, *92*, 251902–1-251902–3.
[41] J. Biener, G. W. Nyce, A. M. Hodge, M. M. Biener, A. V. Hamza, S. A. Maier, *Adv. Mater.* **2008**, *20*, 1211–1217.
[42] J. Weissmüller, R. C. Newman, H.-J. Jin, A. M. Hodge, J. W. Kysar, *MRS Bull.* **2009**, *34*, 577–586.
[43] X. Y. Lang, P. F. Guan, L. Zhang, T. Fujita, M. W. Chena, *Appl. Phys. Lett.* **2010**, *96*, 073701–1-073701–3.
[44] D. Rakic, A. B. Djurisic, J. M. Elazar, M. L. Majewski, *Appl. Opt.* **1998**, *37*, 5271–5283.
[45] S. Link, M. B. Mohamed, M. A. El-Sayed, *J. Phys. Chem. B* **1999**, *103*, 3073–3077.
[46] C. L. Nehl, H. W. Liao, J. H. Hafner, *Nano Lett.* **2006**, *6*, 683–688.

Submitted to ADVANCED MATERIALS

Supporting Information

Well-Defined Multibranched Gold with Surface Plasmon Resonance in Near-Infrared Region from Seeding Growth Approach Using Gyroid Block Copolymer Template

By *Han-Yu Hsueh, Hung-Ying Chen, Yu-Chueh Hung, Yi-Chun Ling, Shangjr Gwo,and Rong-Ming Ho**

[*] Prof. R.-M. Ho
Department of Chemical Engineering, National Tsing Hua University, Hsinchu 30013, Taiwan
Frontier Research Center on Fundamental and Applied Sciences of Matters, National Tsing Hua University, Hsinchu 30013, Taiwan
E-mail: rmho@mx.nthu.edu.tw

Dr. H.-Y. Hsueh
Department of Chemical Engineering, National Tsing Hua University, Hsinchu 30013, Taiwan

Dr. H.-Y. Chen, Prof. Dr. S. Gwo
Department of Physics, National Tsing Hua University, Hsinchu 30013, Taiwan

Mr. Y.-C. Ling, Prof. Dr. Y.-C. Hung
Institute of Photonics Technologies, National Tsing Hua University, Hsinchu 30013, Taiwan

Synthesis of PS-PLLA BCPs

The PS-PLLA was prepared by a sequential living polymerization using a double-headed initiator. Detailed synthetic routes of the PS-PLLA sample were described in our previously published results.[1,2] The number-average molecular weight and the molecular weight distribution (i.e., polydispersity index) of the PS were determined by GPC. The polydispersity index (PDI) of PS-PLLA was determined by GPC and the numbers of L-LA repeating units versus styrene repeating units were determined by ^{1}H NMR analysis. The number-average molecular weights of the PS, the PLLA and the PDI of the PS-PLLA are 34000 g mol^{-1}, 27000 g mol^{-1} and 1.21, respectively. The volume fraction of PLLA, f_{PLLA}^{v}, is thus calculated as 0.39 by assuming the densities of PS and PLLA are 1.02 and 1.248 g cm^{-3}, respectively.

Sample Preparation

Bulk samples of PS-PLLA were prepared by solution casting from dichloromethane (CH_2Cl_2) solution (10 wt % of PS-PLLA with PLLA volume fraction, f_{PLLA}^{v}=0.39) at room temperature for two weeks, and then dried in a vacuum oven at 65^{o}C for three days. The dry samples were first heated to the maximum annealing temperature, T_{max}=185^{o}C for three minutes to eliminate the PLLA crystalline residues that were formed during the preparation procedure. After quenching from the microphase-separated, ordered melt at 185^{o}C, the samples were prepared for SAXS experiments and then sectioned by ultra-microtome (thickness ~ 100 nm) for TEM observation. The microsections were stained by exposing to the vapor of a 4% aqueous RuO_4 solution for one hour. The RuO_4 attacks the double bonds in the PS blocks, rendering those microphase-separated domains dark in TEM due to the mass-thickness contrast. Then, the PLLA blocks of the PS-PLLA bulk samples were removed by hydrolysis, using a 0.5M basic solution that was prepared by dissolving 2g of sodium hydroxide in a 40/60 (by volume) solution of methanol/water. After three days of hydrolysis,

the hydrolyzed samples were rinsed using a mixture of DI water and methanol, and then used as templates for following seeding growth approach.

Seeding Growth Approach

The nanoporous PS template with interconnected tortuous air network was soaked in an seeding aqueous solution mixed with methanol (20 mL) and $HAuCl_4 \cdot 3H_2O$ (0.01~0.1g) with stirring at room temperature for several hours (3~4 hrs). After washing gently with methanol/H_2O solution to remove redundant Au ions covering on sample surfaces, the pore-filled samples were immersed into a hydrazinium hydroxide (100 %, hydrazine 85 %)/methanol solution for the nucleation of Au. The diameter of Au nuclei is around 25~30 nm. By controlling the concentration of Au ions, the nucleation density of Au can be well defined. With the control of low enough Au ion concentrations, suitable amount of Au nuclei within the nanochannels of the template can be formed. Subsequently, a fresh growth solution consisting of $HAuCl_4$. $3H_2O$ (0.05g), diethanolamine (DEA, 0.1g), HCl (1N, 0.1 mL), and methanol (20 ml) was prepared and then the pre-treated template with low content of Au nuclei was immersed into the prepared solution. Accordingly, Au ions were reduced to Au clusters arising from pre-formed Au nuclei so as to gradually develop within the nanochannels through the growth process and eventually form the PS/Au nanohybrids with preserved gyroid texture. The PS/Au nanohybrids were sectioned by Leica Ultra-microtome (thickness ~ 200 nm) at room temperature for the measurement of UV-Vis absorption spectra. The microsections were collected on quartz.

Degeneration for PS Template

To produce the nanostructured Au materials, the PS template of the PS/Au nanohybrids was degraded by exposure to UV. The degradation was carried out under atmosphere conditions for 24h using a UV source. The intensity of the UV source was tuned for the efficient degradation of the PS matrix and did not affect the templated texture of the inorganic

Au nanostructures. Exposure was to UV with a wave length of 254 nm and an intensity of 3mW/cm^2. Consequently, the nanostructured Au materials were easily obtained. In addition, UV-ozonolysis is a suitable method for degeneration of thicker PS templates without destroying the Au nanostructures.

Field-Emission Scanning Electron Microscopy (FESEM)

FESEM observations were performed on a JEOL JSM-6700F using accelerating voltages of 1.5-3 keV. Before observations, the samples were sputter-coated with 2-3 nm of platinum to avoid the charge effect (the platinum coating thickness was estimated from a calculated deposition rate and experimental deposition time).

Small-angle X-ray (SAXS)

Small-angle X-ray scattering (SAXS) experiments were conducted at the synchrotron X-ray beam-line BL23A at the National Synchrotron Radiation Research Center (NSRRC) in Hsinchu. The wavelength of the X-ray beam was 0.155 nm. The incident X-ray beam was focused vertically by a mirror and monochromated to the energy of 10 keV by a germanium (111) double-crystal monochromator. The wavelength of the X-ray beam was 1.24 Å. The beam stop was a round tantalum disk with 4 mm in diameter. A MAR CCD X-ray detector (MAR USA) was used to collect the two-dimensional (2D) SAXS patterns. One-dimensional (1D) linear profile was obtained by integration of the 2D pattern. The scattering angle of the SAXS patter was calibrated using silver behenate, with the first-order scattering vector q^* ($q^* = 4\lambda^{-1} \sin\theta$, where 2θ is the scattering angle) being 1.076 nm^{-1}.

Wide-angle X-ray Scattering (WAXS)

To further confirm the crystalline structure of the nanostructured Au materials, we collected the powder of nanostructured Au and performed a XRD experiment. The crystalline structure of the as-prepared product was characterized by XRD using a Rigaku Dmax 2200 X-

ray diffractometer with Cu KR radiation (λ= 0.1542 nm). The scanning 2θ angle ranged between 20° and 120° with a step scanning of 1° for 1 s.

Identification of Gyroid Phase

A DG phase consisting of co-continuous PLLA networks in a PS matrix can be formed after solution casting of the synthesized PS-PLLA followed by quenching from the microphase-separated melt. One-dimensional small-angle X-ray scattering (1D SAXS) profile (**Fig. S1a**) confirms the DG phase with a space group of $Ia\bar{3}d$ at which the scattering peaks are found at q* ratios of $\sqrt{6}:\sqrt{8}:\sqrt{14}:\sqrt{16}$. The first intensity maximum is centered at q = 0.154 nm^{-1}, corresponding to the d_{211} spacing equal to 40.7 nm and the lattice parameter "*a*" of 100 nm ($a = \sqrt{6}\, d_{211}$). After hydrolytic treatment, the PLLA networks can be selectively removed to give a PS matrix possessing interconnected air networks as a template for the nucleation and growth of Au through seeding growth approach. **Figure S1b** displays the 1D SAXS profile of the PS-PLLA after hydrolysis; the diffraction peaks at q* ratios remain unchanged as compared to **Figure S1a**, reflecting the formation of DG nanochannels. The corresponding TEM image (**Fig. S2a**) of the microsection of solution-cast PS-PLLA sample further confirms the observed gyroid phase, and the nanoporous PS template with gyroid-forming nanochannels can be observed as shown in **Figure S2b**.

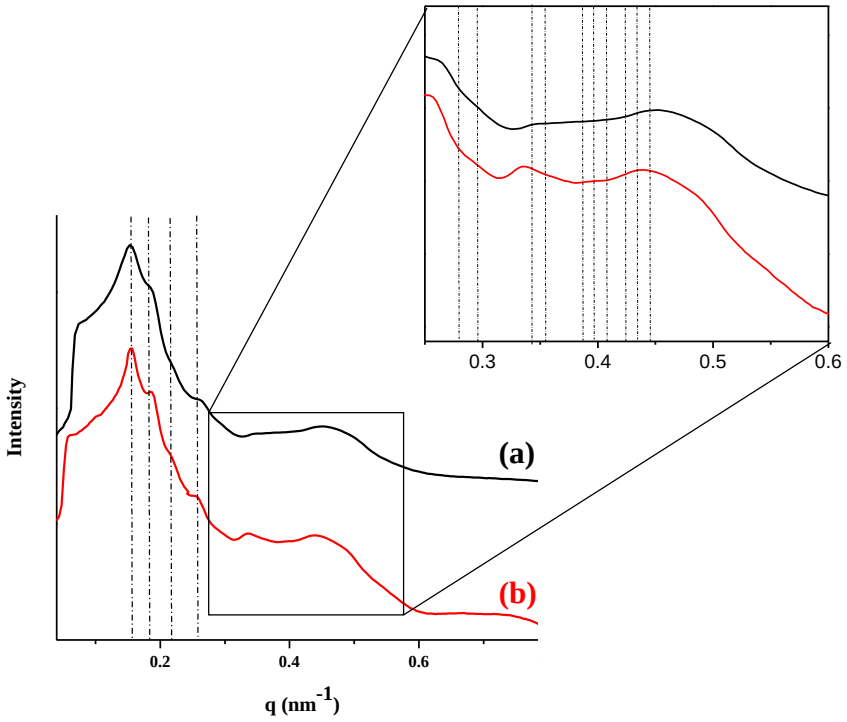

Figure S1. One-dimensional SAXS profiles of a) gyroid-forming PS-PLLA after thermal treatment. The interdomain spacing of $(211)_{gyroid}$ ($d_{(211)G}$) was determined as approximately 40.7 nm from the primary reflection; b) nanoporous PS template form the gyroid-forming PS-PLLA after removal of minor PLLA networks. The interdomain spacing of $(211)_G$ (i.e., $d_{(211)G}$) of the nanoporous PS template was determined to be approximately 39.8 nm from the primary reflection, indicating that there is a 2.6% shrinkage of its original size. On the basis of the form and structure factors for the double gyroid, characteristic reflections with q ratios of $\sqrt{6} : \sqrt{8} : \sqrt{14} : \sqrt{16} : \sqrt{20} : \sqrt{22} : \sqrt{24} : \sqrt{26} : \sqrt{30} : \sqrt{32} : \sqrt{38} : \sqrt{40} : \sqrt{42} : \sqrt{46} : \sqrt{48} : \sqrt{50}$ are discernible. The expected peaks for an $Ia\bar{3}d$ cubic lattice are indicated by vertical lines.

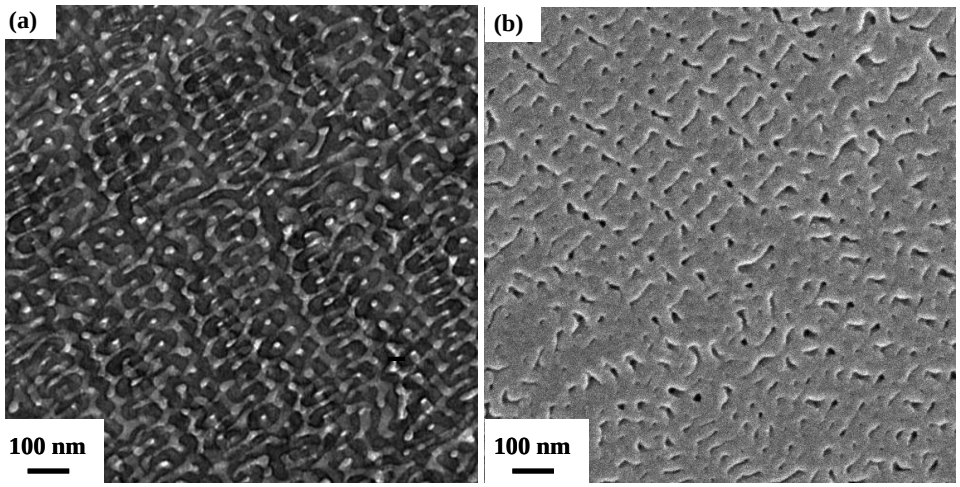

Figure S2. a) TEM micrograph of the [211] projection of the gyroid-forming PS-PLLA with RuO_4 staining. b) FESEM micrograph of nanoporous PS template from the gyroid-forming PS-PLLA after removal of minor PLLA networks.[1]

Preparation of Au Growth Solution

The nanoporous PS template is soaked in an aqueous Au ion (Au^{+3}) solution mixed with methanol. Methanol is used to enhance the wetting tendency of the precursor solution into the PS templates through capillary force. The porous template with the pores filled with Au ion solution is then immersed into a mixed aqueous solution of methanol and hydrazinium hydroxide (N_2H_5OH) (a strong reducing agent for the Au ions) at room temperature. However, the Au clusters with oversized dimension will precipitate immediately, resulting in the blocking of the nanochannels for templating as shown in **Figure S3a**. The growth solution containing Au ions will rapidly become milky as shown in **Figure S3b** due to the formation of Au clusters with a size larger than the wavelength of visible light (namely, much larger than the pore size of the PS template).

To achieve the successful templating, it is necessary to introduce the metal ions in advance to the occurrence of metal deposition so as to carry out templated seeding growth approach for the formation of nanostructured metals. Therefore, how to maintain a low reaction rate and minimize self-nucleation events in the growth process of Au will be critical. It is well-known that precious metals, such as Au, Ag, Pt, and Pd, possess high reduction potential so that the metal ions can be reduced to metal clusters by reducing agent easily. To acquire a transparent and steady growth solution with coexistence of Au ions and reducing agents, weak reducing agents (i.e., DEA) are used (**Fig. S3c**).

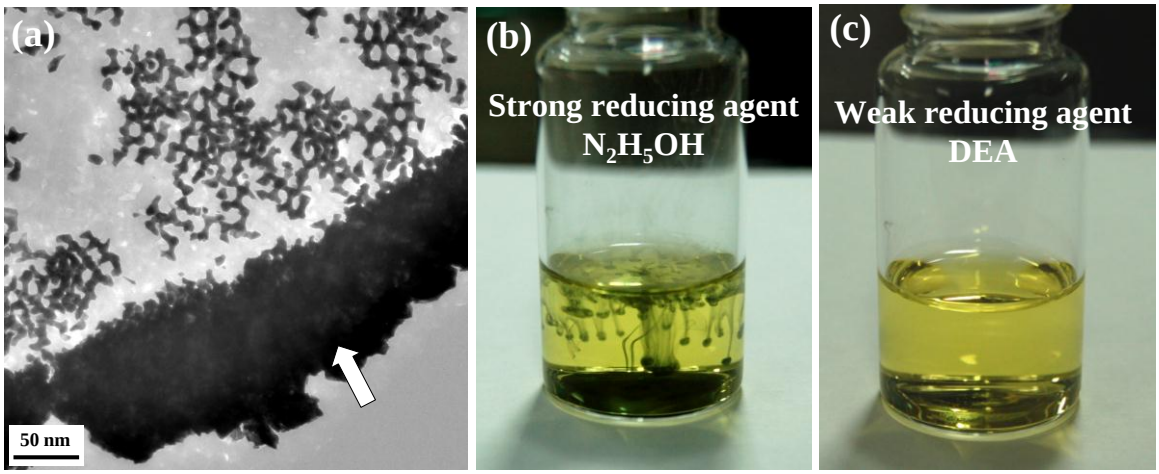

Figure S3. a) TEM images of PS/Au nanohybrids synthesized *via* growth process of Au using N_2H_5OH as a reducing agent. The growth of oversize Au clusters as indicated by a white arrow results in the blocking of the pore-filling process. The images of the growth solution of Au by using b) N_2H_5OH and c) DEA as a reducing agent, respectively.

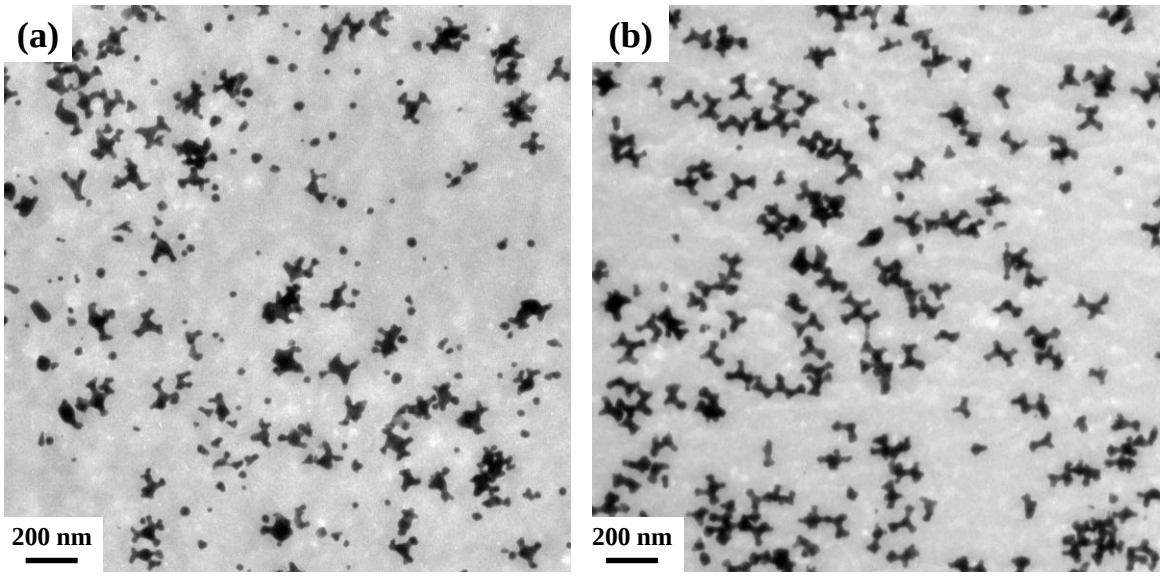

Figure S4. TEM images of a) Au spheres and branched Au from the nucleation of Au without the addition of chloride ions; b) Heterogeneous growth of branched Au nanostructures from the nucleation of Au with the addition of chloride ions.

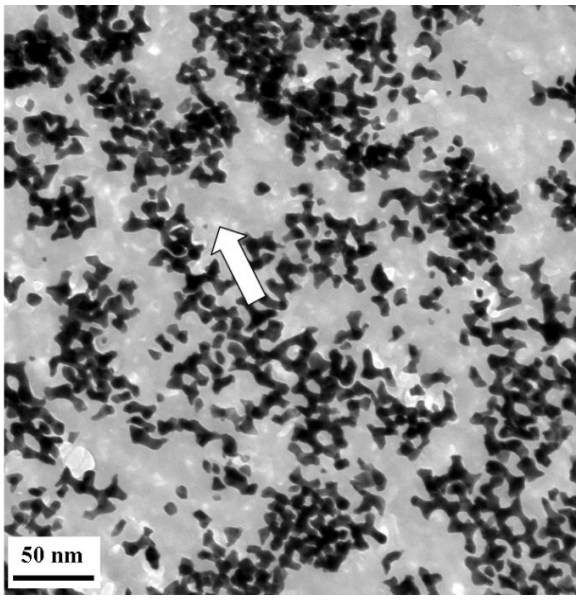

Figure S5. TEM image of the clusters of Au nanostructures (i.e., 3DON Au particles) with different size in dimension. The area with remaining nanochannels as indicated by a white arrow is caused by the limited diffusion due to the blocking described above.

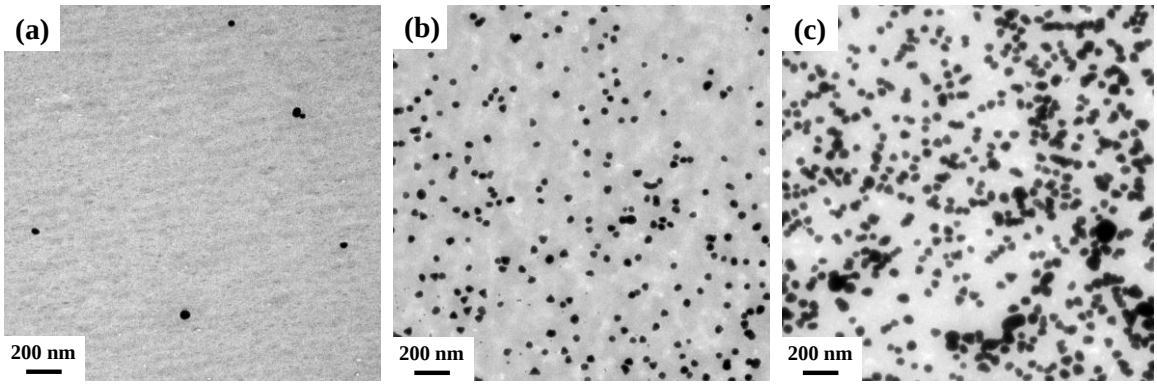

Figure S6. TEM images of Au NPs (Au nuclei) from nucleation of Au (III) ions within the BCP template *via* seeding growth approach with different Au ion concentrations: a) 50 ppm, and the nucleation density is estimated as 2.5×10^4 nuclei per cubic centimeter (cm^3). b) 500 ppm, and the nucleation density is estimated as 7.0×10^6 nuclei per cubic centimeter (cm^3). c) 1500 ppm $HAuCl_4$ in methanol.

Simulation of Mie Theory for Au Spheres in PS matrix

Note that a typical Au nanosphere has a LSPR wavelength around 520 nm in water but the behavior of LSPR will be affected by the size of Au NPs as well as refractive index of the environment. Therefore, the Mie theory simulator was further performed to confirm the absorption frequency for 28 nm Au nanospheres surrounded by a dielectric medium with the refractive index of 1.55 (the refractive index of PS). The simulation result from Mie theory is also well consistent with the experimental and simulated results as shown in **Figure S7**, indicating the optical measurement and analysis of nanostructured Au are reliable.

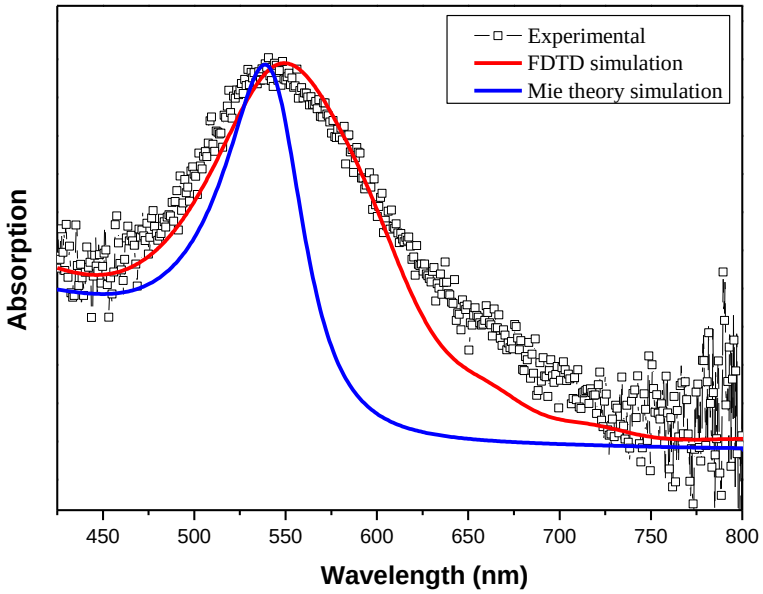

Figure S7. UV-Vis absorption spectra (blank squares), FDTD simulation (red line), and Mie theory simulation (blue line) of Au NPs with 28 nm in diameter within the PS template. A single LSPR peak at a wavelength of 538 nm can be observed.

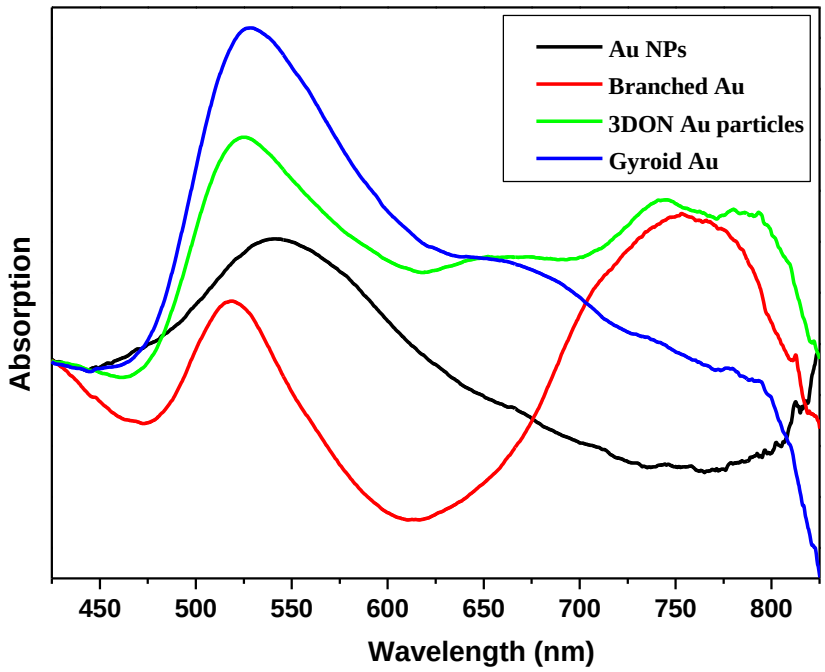

Figure S8. UV-Vis absorption spectra of various nanostructured Au materials including Au NPs, branched Au, 3DON Au particles, and gyroid Au within the PS template with thickness of 200 nm *via* templated seeding growth approach. Note that the spectra are smoothed and vertically shifted for display purposes so that absolute peak height is not proportional to the absorbance.

References

_[1] H. Y. Hsueh, R. M. Ho, *Langmuir* **2012**, *28*, 8518-8529.

_[2] H. Y. Hsueh, Y. C. Huang, R. M. Ho, C. H. Lai, T. Makida, H. Hasegawa, *Adv. Mater.* **2011**, *23*, 3041-3046.